Polaron Formation in the Presence of Rashba Spin-Orbit Coupling: Implications for Spintronics

Lucian Covaci and Mona Berciu

Department of Physics and Astronomy, University of British Columbia, Vancouver, British Columbia, Canada, V6T 1Z1

(Received 23 February 2009; published 8 May 2009)

We study the effects of the Rashba spin-orbit coupling on polaron formation, using a suitable generalization of the momentum average approximation. While previous work on a parabolic band model found that spin-orbit coupling increases the effective mass, we show that the opposite holds for a tight-binding model, unless both the spin-orbit and the electron-phonon couplings are weak. It is thus possible to lower the effective mass of the polaron by increasing the spin-orbit coupling. We also show that when the spin-orbit coupling is large as compared to the phonon energy, the polaron retains only one of the spin-polarized bands in its coherent spectrum. This has major implications for the propagation of spin-polarized currents in such materials, and thus for spintronic applications.

DOI: 10.1103/PhysRevLett.102.186403 PACS numbers: 71.38.−k, 71.70.Ej

Spintronics is focused on finding ways to efficiently manipulate the spin of electrons [1]. A widely investigated approach is to lift the spin degeneracy using spin-orbit coupling (SO), such as the Rashba SO coupling of a confined system whose quantum well lacks inversion symmetry [2]. Experimentally, the Rashba effect is seen in many systems, e.g., semiconductor heterostructures like GaAs and InAs, surface states of metals like Au(111) [3], and surface alloys like Bi/Ag [4] or Pb/Ag [5].

Confined two-dimensional systems may also couple strongly to optical phonons of the substrate. Tuning of these electron-phonon (e-ph) interactions was shown to be experimentally viable in organic single-crystal transistors [6]. Strong e-ph coupling is interesting because it leads to polaron creation, whereas the coherent quasiparticle is an electron surrounded by a phonon cloud. The polaron dispersion and effective mass can be significantly renormalized from those of the bare band electron [7].

An interesting question is whether the e-ph and the SO coupling can be used in conjunction to tailor differently the properties of the two bands with different spin. The interplay between Rashba SO and e-ph couplings has been studied for systems with parabolic bands and weak e-ph coupling, using the self-consistent Born approximation [8]. The main conclusion was that SO enhances the effective e-ph coupling due to an effectively reduced dimensionality of the low-energy density of states. (Such mass enhancements also appear for correlated electrons [9,10].) In this Letter, we investigate this problem using a suitable generalization of the momentum average (MA) approximation [11], which allows us to study tight-binding (nonparabolic) models for any e-ph coupling strength. This is because this method is accurate for all coupling strengths, and becomes exact for both very weak and very strong couplings. We find that except at weak couplings, the conclusions of Ref. [8] do not apply for a tight-binding dispersion. To the contrary, the effective e-ph coupling is suppressed by SO coupling. We also calculate spin-dependent spectral functions and show that in a certain regime, the coherent polaron band is dominated by contributions from only one SO electronic band (the "−" band). This has major implications for spin-dependent transport, allowing for the possibility to manipulate the effective mass and the spin polarization of quasiparticles by tuning the e-ph and SO couplings.

Consider a single electron on a two-dimensional square lattice with SO coupling, which also interacts with optical phonons of energy Ω ($\hbar = 1$) via Holstein e-ph coupling [12]. Its Hamiltonian is written in terms of $\mathbf{k}$-space spinors as

$$\mathcal{H} = \sum_{\mathbf{k}} (c^\dagger_{\mathbf{k}\uparrow} c^\dagger_{\mathbf{k}\downarrow}) \begin{pmatrix} \epsilon_{\mathbf{k}} & \phi_{\mathbf{k}} \\ \phi^*_{\mathbf{k}} & \epsilon_{\mathbf{k}} \end{pmatrix} \begin{pmatrix} c_{\mathbf{k}\uparrow} \\ c_{\mathbf{k}\downarrow} \end{pmatrix} + \Omega \sum_{\mathbf{q}} b^\dagger_{\mathbf{q}} b_{\mathbf{q}} + \frac{g}{\sqrt{N}} \sum_{\mathbf{k},\mathbf{q}} (c^\dagger_{\mathbf{k}-\mathbf{q}\uparrow} c^\dagger_{\mathbf{k}-\mathbf{q}\downarrow}) \begin{pmatrix} b^\dagger_{\mathbf{q}} + b_{-\mathbf{q}} & 0 \\ 0 & b^\dagger_{\mathbf{q}} + b_{-\mathbf{q}} \end{pmatrix} \begin{pmatrix} c_{\mathbf{k}\uparrow} \\ c_{\mathbf{k}\downarrow} \end{pmatrix},$$

where $\epsilon_{\mathbf{k}} = -2t[\cos(k_x a) + \cos(k_y a)]$ is the two-dimensional nearest-neighbor hopping free-electron dispersion and the Rashba SO coupling is $\phi_{\mathbf{k}} = 2V_s[i \sin(k_x a) + \sin(k_y a)]$. Different dispersions and/or SO couplings can be studied similarly. As usual, $c^\dagger_{\mathbf{k},\sigma}$ is the creation operator for an electron with momentum $\mathbf{k}$ and spin σ, while $b^\dagger_{\mathbf{q}}$ creates a phonon of momentum $\mathbf{q}$. Both electron spin channels interact with the phonons through the local lattice displacement, with an e-ph coupling constant g. The lattice has a total of N sites, where $N \to \infty$, and periodic boundary conditions. Momentum sums are over the Brillouin zone.

The 2×2 Green's functions for the noninteracting system (with no e-ph coupling) are defined as

$$\bar{G}_0(\mathbf{k}, \omega) = \langle 0 | \begin{pmatrix} c_{\mathbf{k}\uparrow} \\ c_{\mathbf{k}\downarrow} \end{pmatrix} \hat{G}_0(\omega) (c^\dagger_{\mathbf{k}\uparrow} c^\dagger_{\mathbf{k}\downarrow}) | 0 \rangle = \begin{pmatrix} G_{0+}(\mathbf{k}, \omega) & e^{i\xi_{\mathbf{k}}} G_{0-}(\mathbf{k}, \omega) \\ e^{-i\xi_{\mathbf{k}}} G_{0-}(\mathbf{k}, \omega) & G_{0+}(\mathbf{k}, \omega) \end{pmatrix}, \quad (1)$$

where the symmetric and antisymmetric Green's functions are given by

$$G_{0\pm}(\mathbf{k},\omega)=\frac{1}{2}\Big(\frac{1}{\omega+i\eta-\epsilon_k+|\phi_k|}\pm\frac{1}{\omega+i\eta-\epsilon_k-|\phi_k|}\Big),$$

$\hat{G}_0(\omega)=[\omega-\mathcal{H}_0+i\eta]^{-1}$ is the resolvent corresponding to $\mathcal{H}_0=\mathcal{H}|_{g=0}$, and the phase factor is $\xi_{\mathbf{k}}=\phi_{\mathbf{k}}/|\phi_{\mathbf{k}}|$. To avoid confusion with scalars, all 2×2 matrices will be identified by a bar, such as in the $\bar{G}_0(\mathbf{k},\omega)$ notation.

The full Green's function, defined as usually

$$\bar{G}(\mathbf{k},\omega)=\langle 0|\begin{pmatrix}c_{\mathbf{k}\uparrow}\\ c_{\mathbf{k}\downarrow}\end{pmatrix}\hat{G}(\omega)(\,c^\dagger_{\mathbf{k}\uparrow}c^\dagger_{\mathbf{k}\downarrow}\,)|0\rangle, \tag{2}$$

can in principle be calculated exactly by applying the equation of motion method. The full Green's function can be related to the noninteracting one by using the Dyson equation, $\hat{G}(\omega)=\hat{G}_0(\omega)+\hat{G}(\omega)V\hat{G}_0(\omega)$—here $V=\mathcal{H}-\mathcal{H}_0$ is the e-ph interaction. As shown previously for the Holstein Hamiltonian [11,13,14], the repeated use of the Dyson identity generates a system of equations involving generalized Green's functions with various numbers of phonons. In the presence of SO interactions, the equations of motion are similar, except they are in terms of 2×2 Green's functions. As a result, we can implement the MA approximations in the same way, and all conclusions regarding accuracy for all e-ph coupling strengths, sum rules obeyed exactly by the spectral weight, etc., remain true. A somewhat analogous procedure was used to compute the 2×2 Green's function describing rippled graphene [15]; however, there the matrices are related to different sublattices, not to different spin projections.

For all levels of the MA approximation, the Green's function can be written in the standard form:

$$\bar{G}(\mathbf{k},\omega)=[\bar{G}_0(\mathbf{k},\omega)^{-1}-\bar{\Sigma}(\mathbf{k},\omega)]^{-1}, \tag{3}$$

where the self-energy $\bar{\Sigma}(\mathbf{k},\omega)$ has different expressions depending on the level of MA approximation used. For the simplest, least accurate MA$^{(0)}$ level [11,13], the self-energy has no $\mathbf{k}$ dependence and is given by an infinite continued fraction $\bar{\Sigma}_{\mathrm{MA}^{(0)}}(\omega)=g^2\bar{A}_1(\omega)$, defined by

$$\bar{A}_n(\omega)=n\bar{g}_0(\omega-n\Omega)[\mathbb{1}-g^2\bar{g}_0(\omega-n\Omega)\bar{A}_{n+1}(\omega)]^{-1}, \tag{4}$$

where

$$\bar{g}_0(\omega)=\frac{1}{N}\sum_{\mathbf{k}}\bar{G}_0(\mathbf{k},\omega)=\begin{pmatrix}g_{0+}(\omega) & 0\\ 0 & g_{0+}(\omega)\end{pmatrix} \tag{5}$$

is the momentum average of the noninteracting Green's function over the Brillouin zone. Note that because the off-diagonal part is antisymmetric, its average over the Brillouin zone vanishes; i.e., $\bar{g}_0(\omega)$ and all $\bar{A}_n(\omega)$ matrices are diagonal.

As discussed extensively in Refs. [13,14], MA$^{(0)}$ is accurate for ground state properties, but it fails to properly predict the polaron + one phonon continuum. As a result, it overestimates the polaron bandwidth. This problem is fixed at the MA$^{(1)}$ level, where a phonon is allowed to appear away from the polaron cloud. For the Holstein model (and by extension, in the presence of SO coupling) both these approximations predict $\mathbf{k}$-independent self-energies. Here, they are diagonal as well; i.e., phonon emission or absorption is not allowed to scatter the electron between the spin-polarized bands. Of course these are approximations, although it is worth noting that all non-crossed diagrams are diagonal and $\mathbf{k}$-independent. This is why the self-consistent Born approximation predicts a self-energy that is also $\mathbf{k}$-independent and diagonal [8].

In MA, however, the effect of noncrossed diagrams is included for MA$^{(2)}$ and higher levels (in variational terms, these allow two or more phonons to appear far from the polaron cloud, and the order of their emissions and absorptions is relevant). We therefore report MA$^{(2)}$ results here. Following a similar procedure to that described in detail in Ref. [14], the MA$^{(2)}$ self-energy is found as

$$\bar{\Sigma}_{\mathrm{MA}^{(2)}}(\mathbf{k},\omega)=\bar{x}(0), \tag{6}$$

given by the solution of the system of coupled equations for the unknown 2×2 matrices $\bar{x}(i)$:

$$\sum_j\bar{M}_{i,j}(\mathbf{k},\omega)\bar{x}(j)=e^{i\mathbf{k}\mathbf{R}_i}g^2\bar{G}_0(-i,\tilde{\tilde{\omega}}). \tag{7}$$

The sum is over lattice sites $i=(i_x,i_y)$ located at $\mathbf{R}_i=i_xa\hat{x}+i_ya\hat{y}$. The 2×2 matrices $\bar{M}_{i,j}(\mathbf{k},\omega)$ are

$$\bar{M}_{00}=\mathbb{1}-g^2\bar{g}_0(\tilde{\omega})\bar{g}_0(\tilde{\tilde{\omega}})(2\bar{a}_{31}^{-1}-\bar{a}_{21}^{-1}), \tag{8}$$

$$\bar{M}_{i0}=-g^2\bar{g}_0(\tilde{\omega})e^{i\mathbf{k}\cdot\mathbf{R}_i}\bar{G}_0(-i,\tilde{\tilde{\omega}})(2\bar{a}_{31}^{-1}-\bar{a}_{21}^{-1}) \tag{9}$$

for $i\neq 0$, and for both $i,j\neq 0$:

$$\bar{M}_{ij}=\bar{a}_{21}\delta_{i,j}\mathbb{1}-g^2e^{i\mathbf{k}\cdot\mathbf{R}_i}\bar{G}_0(j,\tilde{\omega})[(\bar{A}_2-\bar{A}_1)\delta_{i,-j}+\bar{G}_0(-i-j,\tilde{\tilde{\omega}})\bar{a}_{21}^{-1}]. \tag{10}$$

Here we defined $\bar{a}_{ij}=\mathbb{1}-g^2\bar{g}_0(\tilde{\omega})(\bar{A}_i-\bar{A}_j)$, where $\bar{A}_1\equiv\bar{A}_1(\omega-2\Omega)$, $\bar{A}_2\equiv\bar{A}_2(\omega-\Omega)$, $\bar{A}_3\equiv\bar{A}_3(\omega)$ are continuous fractions defined by Eq. (4), and $\tilde{\omega}=\omega-2\Omega-g^2\bar{A}_1|_{(1,1)}$, $\tilde{\tilde{\omega}}=\omega-g^2\bar{g}_0(\tilde{\omega})|_{(1,1)}(\bar{a}_{21}^{-1})|_{(1,1)}$ [since the $\bar{A}$, $\bar{a}$, $\bar{g}_0$ matrices are proportional to $\mathbb{1}$, the (2,2) diagonal matrix element can be used just as well in the definitions of $\tilde{\omega}$, $\tilde{\tilde{\omega}}$]. Finally, the real space Green's functions appearing in the inhomogeneous terms are given, as usual, by

$$\bar{G}_0(i,\omega)=\frac{1}{N}\sum_{\mathbf{k}}e^{i\mathbf{k}\mathbf{R}_i}\bar{G}_0(\mathbf{k},\omega). \tag{11}$$

It is important to note that for $i\neq 0$, $\bar{G}_0(i,\omega)$ acquires off-diagonal components, which lead to off-diagonal contributions in $\bar{\Sigma}_{\mathrm{MA}^{(2)}}(\mathbf{k},\omega)$. Since below the free-electron continuum $\bar{G}_0(i,\omega)$ decreases exponentially as $|\mathbf{R}_i|$ increases,

the system in Eq. (7) can be truncated at a small $|i|$. We truncate at $|\mathbf{R}_i| \simeq 10a$, such that the relative error of the spectral function is less than 10^{-3}.

Once the self-energy is known, the full Green's function is calculated and in turn provides accurate estimates for spectral weights, ground state energy, effective mass, etc. In the noninteracting case ($g = 0$) the ground state with energy $E_0 = -4t\cos(k_{\min}) - V_s\sqrt{8}|\sin(k_{\min})|$ consists of four degenerate points in $\mathbf{k}$ space $(\pm k_{\min}, \pm k_{\min})$, where $k_{\min} = \arctan[V_s/(\sqrt{2}t)]$. On the other hand, in the absence of SO coupling ($V_s = 0$), as the effective e-ph coupling $\lambda = g^2/(4t\Omega)$ is turned on, there is a crossover from a light, large-polaron to a very heavy, small polaron at $\lambda \sim 1$. In Fig. 1 we show the ground state energy measured from E_0 for weak, medium, and strong effective e-ph couplings, as a function of the Rashba SO coupling. For large SO coupling, the renormalization of the energy and effective mass (shown in the inset) is strongly suppressed, indicating light polarons even when $\lambda = 2$. This is in contrast with reported results for a parabolic band [8], which are based on the fact that their density of states at the band edge have a square root singularity, because in a continuum model the locus of momenta defining the ground state is a circle of radius $k_{\min}$. This is not true for a tight-binding dispersion, where the van Hove singularity is shifted from the 4-point degenerate ground state to higher energies. Actually, as expected, the results for the parabolic band agree with our tight-binding results if both λ and V_s/t are very small. Indeed, for $\lambda = 0.75$, the effective mass increases slightly with V_s at small V_s, before decreasing at larger V_s values. Such behavior is more apparent as $\lambda \to 0$ [16].

Our results can be understood by noting that the free-electron bandwidth increases with increasing V_s. This results in an effective e-ph coupling, which compares the polaron binding energy to this renormalized bandwidth, that effectively decreases. As a result, away from the limit where both λ and V_s/t are very small, an increase in the SO coupling leads to a drop in the effective mass, making it possible to tune the mass of the polaron between heavy and light. Light polarons are thus found either for small λ irrespective of V_s/t or at large λ and large enough V_s/t. As we show next, however, their nature and spin character may be very different.

The MA$^{(2)}$ approximation is quantitatively accurate not only for low but also for high energy states, as it satisfies exactly the first 10 spectral weight sum rules and with good accuracy all other ones [14]. It is thus possible to have an accurate depiction of the high energy states by calculating a spin-dependent spectral function:

$$\vec{A}(\mathbf{k}, \omega) = -\frac{1}{\pi}\,\mathrm{Im}(\mathrm{Tr}[\vec{\sigma}\,\bar{G}(\mathbf{k}, \omega)]), \tag{12}$$

where $\vec{\sigma}$ are the Pauli matrices. The direction of $\vec{A}(\mathbf{k}, \omega)$ gives the direction of the expectation value of the spin, while its magnitude gives the density of states with momentum $\mathbf{k}$. We know that in the noninteracting case as we go around the Γ point, eigenstates have spin perpendicular to their momentum direction and rotate clockwise for one band and anticlockwise for the other. For the coupled system we observe similar spin eigenstates and thus choose to plot the following quantity:

$$\tilde{A}(\mathbf{k}, \omega) = [\vec{u}_k \times \vec{A}(\mathbf{k}, \omega)] \cdot \vec{u}_z, \tag{13}$$

where $\vec{u}_k$ and $\vec{u}_z$ are unit vectors parallel to $\mathbf{k}$, respectively z axis. The two spin-polarized bands will now correspond to the opposite signs of $\tilde{A}(\mathbf{k}, \omega)$.

Since the polaron bandwidth cannot exceed Ω, we expect the character of the polaron band to depend on the relation between Ω and the energy difference between the spin-split electron bands. In order to exemplify this we plot $\tilde{A}(\mathbf{k}, \omega)$ in Fig. 2 for $\lambda = 1$, $\Omega = 0.8t$, and $V_s = 0.4t$. The spectral function is shown along the (0, 0)-(π, π) line in order to intersect the ground state at $(k_{\min}, k_{\min})$. In this case $\Omega/(E_0 - 4t) > 1$, and we see two coherent polaron bands corresponding to the two spin polarizations, with

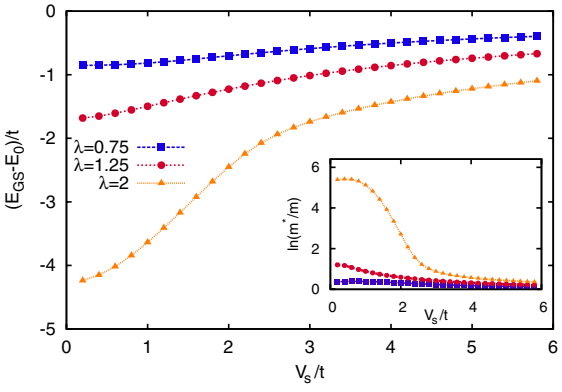

FIG. 1 (color online). The ground state energy as a function of Rashba SO coupling for three values of the e-ph coupling. The inset shows the effective mass on a logarithmic scale as a function of Rashba SO coupling.

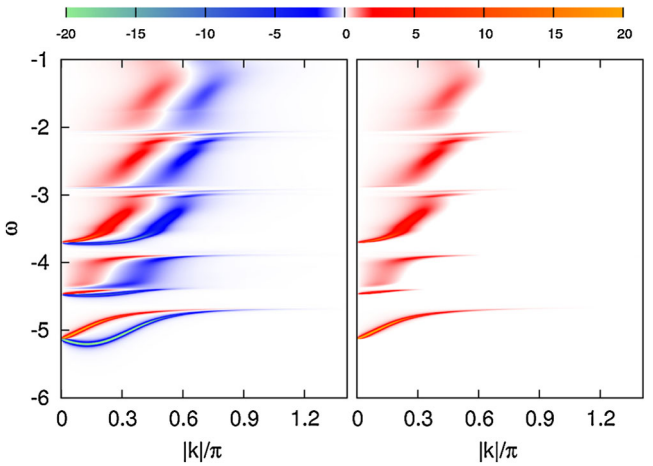

FIG. 2 (color online). Spin-dependent spectral function $\tilde{A}(\mathbf{k}, \omega)$, for $\lambda = 1$, $\Omega = 0.8t$, and $V_s = 0.4t$. The right panel shows only the "+" band for clarity.

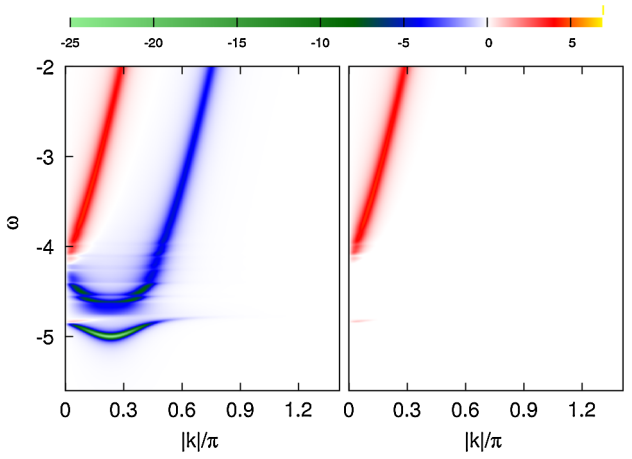

FIG. 3 (color online). Spin-dependent spectral function $\tilde{A}(\mathbf{k}, \omega)$, for $\lambda = 1$, $\Omega = 0.2t$, and $V_s = 0.8t$. The right panel shows only the "+" band for clarity.

similar quasiparticle weights. We conclude that when Ω is larger than the SO splitting, the polaronic quasiparticles are rather similar to the noninteracting electrons, except for the renormalized mass and suppressed quasiparticle weight. Of course, the spectrum above $E_{\mathrm{GS}} + \Omega$ becomes incoherent due to e-ph scattering.

In Fig. 3 we plot $\tilde{A}(\mathbf{k}, \omega)$ for $\lambda = 1.0$, $\Omega = 0.2t$, and $V_s = 0.8t$. Now $\Omega/(E_0 - 4t) < 1$, and because the polaron bandwidth cannot exceed Ω, it is dominated by the low-energy "−" band. There is a large difference between the quasiparticle weights of the two coherent polaron bands (note the different positive and negative scales for the contour plot), and the effective mass of the dominant "−" band is much smaller than that of the low-weight "+" band. Higher energy states have small weights and are highly incoherent, i.e., short-lived.

Consider now injection of a current in such a system. Whereas in a regime like that of Fig. 2 we expect the spin to precess between the two coherent polaronic bands, as it does for noninteracting electrons [17,18], in a regime like in Fig. 3 only the spin component parallel to the "−" band can be efficiently transmitted through the system, which therefore acts as an intrinsic spin polarizer.

This becomes more and more apparent as one moves further into the asymptotic limit where both the SO and the e-ph couplings are large compared to Ω, i.e., $(E_0 - 4t) \gg \Omega$ and $\lambda \gg 1$. In this limit the "−" band in the coherent polaron spectrum becomes lighter and has a higher quasiparticle weight, whereas the "+" band essentially vanishes from the coherent spectrum (its quasiparticle weight is extremely low and its effective mass is extremely large). The resulting light polaron is thus very different from the one we find in the small λ regime, which has both bands in the coherent spectrum with roughly equal quasiparticle weights and effective mass.

This demonstrates that an interplay between SO and e-ph couplings allows indeed for different tailoring of the properties of the two spin-polarized bands, such that one is well described by a long-lived, light quasiparticle while the other is highly incoherent. This will naturally lead to very different conductivities for the two spin polarizations, making such a material ideal as a source and/or detector of spin-polarized currents—these are important components needed for many spintronics applications. These conclusions are based on the use of the MA approximation, which is known to be highly accurate for all e-ph couplings. Moreover, at the MA$^{(2)}$ level we use here, it results in a nondiagonal, $\mathbf{k}$-dependent self-energy; therefore, our results properly include phonon-mediated scattering between the two electronic bands. While our results are for the single electron limit, we expect them to hold for low carrier concentrations where the Fermi energy is the smallest energy scale and many-polaron effects (renormalization of the effective coupling due to overlap of polaron wave functions) are not yet significant [19].

This work was supported by CIFAR Nanoelectronics and NSERC. Discussions with Frank Marsiglio are gratefully acknowledged.

[1] I. Žutić, J. Fabian, and S. Das Sarma, Rev. Mod. Phys. **76**, 323 (2004).
[2] E. I. Rashba, Sov. Phys. Solid State **2**, 1109 (1960).
[3] S. LaShell, B. A. McDougall, and E. Jensen, Phys. Rev. Lett. **77**, 3419 (1996).
[4] C. R. Ast *et al.*, Phys. Rev. Lett. **98**, 186807 (2007).
[5] D. Pacilé *et al.*, Phys. Rev. B **73**, 245429 (2006).
[6] I. H. Hulea *et al.*, Nature Mater. **5**, 982 (2006).
[7] For a review see H. Fehske and S. A. Trugman, in *Polarons in Advanced Materials*, edited by A. S. Alexandrov (Springer-Verlag, Dordrecht, 2007).
[8] E. Cappelluti, C. Grimaldi, and F. Marsiglio, Phys. Rev. B **76**, 085334 (2007); Phys. Rev. Lett. **98**, 167002 (2007); F. Marsiglio (private communications).
[9] A. Ramsak *et al.*, Phys. Rev. B **46**, 14 305 (1992).
[10] A. S. Mishchenko and N. Nagaosa, Phys. Rev. Lett. **93**, 036402 (2004).
[11] M. Berciu, Phys. Rev. Lett. **97**, 036402 (2006).
[12] T. Holstein, Ann. Phys. (N.Y.) **8**, 325 (1959); **8**, 343 (1959).
[13] G. L. Goodvin, M. Berciu, and G. A. Sawatzky, Phys. Rev. B **74**, 245104 (2006).
[14] M. Berciu and G. L. Goodvin, Phys. Rev. B **76**, 165109 (2007); M. Berciu, Phys. Rev. Lett. **98**, 209702 (2007).
[15] L. Covaci and M. Berciu, Phys. Rev. Lett. **100**, 256405 (2008).
[16] L. Covaci and M. Berciu (unpublished).
[17] B. Srisongmuang *et al.*, Phys. Rev. B **78**, 155317 (2008).
[18] C. A. Perroni *et al.*, J. Phys. Condens. Matter **19**, 186 227 (2007).
[19] M. Hohenadler *et al.*, Phys. Rev. B **71**, 245111 (2005).